REPORT DOCUMENTATION PAGE

Form Approved
OMB No. 0704-0188

1. AGENCY USE ONLY (Leave Blank)	2. REPORT DATE	3. REPORT TYPE AND DATES COVERED
	9/3/97	Final Technical Report 6/30/94 - 6/29/97

4. TITLE AND SUBTITLE
"A Study of Impact Ionization and Breakdown Phenomena in SiGe Devices"

5. FUNDING NUMBERS
61103D
3484/TS
AFOSR-TR
97-0391

6. AUTHORS
P. Bhattacharya

7. PERFORMING ORGANIZATION NAME(S) AND ADDRESS(ES)
University of Michigan
Department of Electrical Engineering & Computer Science
1301 Beal Avenue, 2306 EECS Building
Ann Arbor, MI 48109-2122

8. PERFORMING ORGANIZATION REPORT NUMBER

9. SPONSORING / MONITORING AGENCY NAME(S) AND ADDRESS(ES)
AFOSR/NE
110 Duncan Avenue, Suite B115
Bolling AFB, DC 20332-0001

10. SPONSORING / MONITORING AGENCY REPORT NUMBER
F49620-94-1-0404

11. SUPPLEMENTARY NOTES

12a. DISTRIBUTION / AVAILABILITY STATEMENT
Approved for public release; distribution unlimited.

12b. DISTRIBUTION CODE

13. ABSTRACT *(Maximum 200 words)*

The spectral response and impact ionization coefficient ration of $Si_{1-x}Ge_x$ have been determined. Measurements were made on p^+-i-n^+ diodes grown by solid/gas source molecular beam epitaxy. The diodes are characterized by reverse breakdown voltages of 4-12V and dark currents of 20-170pA/μm^2. The long wavelength cut-off of the diodes increases from 1.2μm to 1.6μm as x increases from 0.08 to 1.0 with a maximum responsivity of 0.5 A/W in all the diodes tested. The ratio α/β varies from 3.3 to 0.3 in the same composition range, with $\alpha/\beta=1$ at $x\cong0.45$. These results have important implications in the use of this material system in various photodetection applications. As part of this project we also investigated the problem of high-level n-type doping of Si and SiGe, which is required for high quality diodes.

The use of supersonically injected pulses of phosphine to achieve uniform and high levels of n-type doping in Si during gas-source molecular beam epitaxy was demonstrated. Uniform n-type doping up to levels of $5X10^{19}cm^{-3}$ is obtained. SiGe/Si junction diodes made with this doping technique show good doping profiles and rectifying characteristics.

14. SUBJECT TERMS SiGe, Impact Ionization, Photodiodes

15. NUMBER OF PAGES 21

16. PRICE CODE

17. SECURITY CLASSIFICATION OF REPORT	18. SECURITY CLASSIFICATION OF THIS PAGE	19. SECURITY CLASSIFICATION OF ABSTRACT	20. LIMITATION OF ABSTRACT
UNCLASSIFIED	UNCLASSIFIED	UNCLASSIFIED	UL

I. INTRODUCTION

Photodetectors are important devices for both long-haul and short-distance lightwave network systems for operation in the near infrared region (0.8 to 1.6μm). In addition to optical communication, these devices are also useful for sensing applications. Some of the important performance requirements for these applications are high sensitivity, low noise, wide bandwidth, high reliability and low cost. The avalanche photodiode (APD) is a photodetector with high sensitivity because of its large optical gain resulting from the avalanche multiplication process. With choices of semiconductor materials and optimal device designs, APDs are the most promising high-speed, low-noise detectors for optical communication systems.

In the last two decades, numerous Si APDs have been designed, optimized and commercialized becuase of their versatile and low-cost technology and their reliability. Similarly, Ge photodiodes are also commerically available and provide detection out to ~1.6μm, although these devices exhibit high dark current due to the low bandgap. A considerable amount of work has been done in recent years on the development of $Si_{1-x}Ge_x$ alloys grown on Si substrates [1-4]. Most of the work has focussed on epitaxial growth and characterization of the alloys[5,6] and their application to high-performance heterojunction field effect transistors (HFETs)[7] and heterojunction bipolar transistors(HBTs)[8-10]. With the exception of reports on SiGe/Si superlattice waveguide photodetectors operating at 1.3μm[11-14], little has been reported on the spectral response and impact ionization coefficient of photodiodes suitable for a wide spectral range. The bandgap and bandstructure of the alloys change continuously from Si (x=0) to Ge (x=1). As a consequence, not only will the dark current and spectral response characteristics change, but the impact ionization coefficients are also expected to change due to the changing bandstructure, illustrated in Fig. 1.

The impact ionization process depends largely on the bandstructure and band gap. The ratio of electron (α) and hole (β) impact ionization coefficients is especially important for low noise applications of APDs[15,16] in which, from McIntyre's theory[15], a highly asymmetric ratio α/β is desirable. In Si, α is known to be larger than β with a α/β ratio of 10 ~ 2.5 at 330kV/cm[17-20]. On the other hand, in Ge, α/β equals 0.7 ~ 0.25 [21-23] at the same electric field due to the low hole effective mass which allows the holes to gain energy more easily than in Si. With the exception of a recent theoretical study[24], there is no report on the experimental determination of α and β in pseudomorphic or relaxed $Si_{1-x}Ge_x$ alloys.

In this paper we describe the spectral response and avalanche multiplication characteristics of $Si_{1-x}Ge_x$ photodiodes for the entire composition range $0.08 \leq x \leq 1$. The impact ionization coefficients, α and β have been calculated from measured multiplication coefficients.

II. HIGH LEVEL n-TYPE DOPING WITH SUPERSONIC JET SOURCE

Highly doped semiconductor regions and p-n junctions are required in a variety of applications. In the case of silicon, p-type doping at levels greater than $10^{20}cm^{-3}$ has been easily achieved using solid or gaseous precursors. However, obtaining n-type material at such high concentrations has proven to be very challenging. Solid phosphorus has a very high vapor pressure and hence is not generally used as a dopant source. Some dopants like antimony, which are conventionally employed as solid sources, have a strong tendency to segregate through the film to the surface of the growing layer, acting as surfactants. During molecular beam epitaxy (MBE), Sb doping also suffers from a small and temperature dependent sticking coefficient and strong surface segregation.[25,26] Hence, n-type doping, has been achieved up to $5x10^{18}$ cm^{-3} during MBE only

from gaseous precursors like phosphine (PH_3).[27] Ultrahigh vacuum chemical vapor deposition (UHV-CVD) studies have reported higher levels of incorporation, but with associated changes in surface chemistry and reduced growth rates.[28-32] Also, very high levels of n-doping($<5x10^{19}$ cm^{-3})are presently achieved in the semiconductor industry using ion implantation followed by a high temperature anneal. Alternative techniques need development, as device sizes shrink and low thermal budgets for processing become essential.

During conventional MBE, using thermal molecular or atomic beams with a broad (Gaussian) energy (velocity) distribution, a high substrate temperature is required to provide surface mobility of the arriving adatoms or dopant species. The high substrate temperature provides energy for Sb or P atoms to move from substitutional to interstitial sites and promote surface segregation. If, on the other hand, a high (mono) energetic beam is used instead, then very little surface migration is required for adatoms or dopant species and the substrate temperature can be reduced. We have recently shown[33,34] that low-temperature Si epitaxy is possible by using a disilane source with a supersonic jet. Growth was demonstrated at 450°C, which is much lower than the conventional temperatures of 550°C and above. In this letter we report on the use of supersonic jets of phosphine to achieve uniform and high levels of n-doping during gas-source MBE (GSMBE) of Si.

The growth facility is briefly described. The experiments were conducted in a RIBER-32 gas source MBE system modified to incorporate a pulsed supersonic valve (General Valve Series 9, 0.7 mm nozzle) with an electronic controller. Silicon growth was conducted using disilane at a flow rate of 14 sccm resulting in a chamber pressure of about 3×10^{-6} torr. The dopant is a 1% mixture of phosphine in hydrogen (Voltaix, Inc.) maintained at a source pressure of 1.1 atm. and delivered through the supersonic nozzle at pulse widths (open time) varying from 5 msec to 60 msec. The "off time" was kept constant at 3 seconds. Substrate temperature was varied in the range of 550-650°C. Substrates used were p-type Si (100) wafers (10-20 Ω-cm), cleaned with an initial solvent degreasing followed by a 30 s HF (10%) etch and drying in a N_2 jet before being loaded. Prior to growth, the sample was heated to about 800°C to desorb the native oxide. A buffer silicon epitaxial layer was first grown at $T_s = 650$°C to ensure a smooth starting surface as observed by Reflection High Energy Electron Diffraction (RHEED). Samples were analyzed using Secondary Ion Mass Spectrometry (SIMS), to determine atomic phosphorus concentrations and Spreading Resistance Analysis (SRA) to obtain active dopant levels. Hall measurements were performed using a van der Pauw geometry.

Figure 2(a) shows a plot of phosphorus atomic concentration vs. depth for different pulse widths of the phosphine jet, as measured by Secondary Ion Mass Spectroscopy(SIMS). Concentrations of ~ 10^{19} cm^{-3}, not obtainable using thermal molecular beams, are easily achievable even at substrate temperatures as high as 620°C. As the pulse width is increased, the thickness of film obtained (for a constant growth time) decreases implying a reduction in growth rate. In fact the growth rate is reduced from 160Å/min. under normal growth conditions to 65Å/min. with use of the phosphine supersonic injector. Other groups have reported reduced Si thin film growth rates with increased phosphine injection.[29-32] This results from the adsorption of phosphorus atoms on the Si surface which, in turn, significantly reduces the dissociative chemisorption of Si_2H_4.[35]. Two features are apparent in the data of Fig. 2(a). First, there is a slight amount of dopant surface segregation at a growth temperature of 620°C. Second, the doping level seems to be independent of the supersonic pulse width. We believe that the two features are related; i.e. the high substrate temperature promotes segregation and less phosphorus incorporation. Under these conditions, there is little distinction between a supersonic beam and a thermal beam and there is no advantage

in using a supersonic beam. The data of Fig. 2(b) which shows electrically active phosphorus doping profiles measured by SRA, in samples grown at low temperatures, proves the point. Here, we notice an increase of doping level with decrease of substrate temperature and an absence of surface segregation, indicating that at the low growth temperatures, the supersonic flux provides requisite energy for incorporation into the proper lattice sites.

Table 1 shows results of Hall measurements performed on representative samples using the van der Pauw technique. The thickness of the Hall samples varied from 0.3 to 0.6μm. The Hall mobilities and carrier concentration values obtained are in good agreement with SRA results and published values for electron mobilities in highly doped silicon.[36,37] This suggests that the films are of high electrical quality. Comparison of SIMS and SRA data indicate that the dopant activation is close to 100%.

As discussed earlier, the motivation for this work was to obtain uniform and high levels of dopant incorporation. Figure 3 presents data showing the variation of doping level, measured by SRA, with substrate temperature. Doping levels of 5×10^{19} cm^{-3} have been achieved at a growth temperature of 550°C. This is the first report of such high active carrier concentrations at these temperatures. Other studies have utilized plasma and RF techniques to obtain such levels of doping.[38,39] The increase in doping level with decrease of substrate temperature indicates that the activation of the dopant species from substitutional to interstitial sites is suppressed with lowering of substrate temperature.

Silicon p^+-n^--n^+ and SiGe(p^+)-Si(n^+) diodes were next grown using solid boron from an effusion cell and PH_3/H_2 supersonic jet as the dopant sources. Solid Ge from an effusion cell was used as the Ge source. The diodes were grown on (100) p^+ Si substrates with resistivities of 0.004-0.02 Ω-cm. The p^+-n^--n^+ Si diode consists of a 0.3 μm thick p^+ ($1X10^{18}cm^{-3}$)layer followed by a 0.7 μm n- ($6X10^{15}cm^{-3}$) layer and a 0.7 μm n^+ ($1X10^{19}cm^{-3}$)layer grown at 570°C. The phosphine flow rate was fixed at 1.1 atm and pulses of 3ms separated by 3s off-times were used. The p^+-n^+ diode consists of a 0.5 μm SiGe p+ ($3X10^{18}cm^{-3}$)layer followed by a 0.7 μm n^+ ($6X10^{18}cm^{-3}$)layer, grown at 570°C with the same injector parameters. 84μm diameter mesa diodes were made by photolithography and metallization for the ohmic contacts. The measured doping profiles and the electrical rectifying characteristics of the two types of diodes are illustrated in Figs. 4(a) and (b); excellent rectifying characteristics are obtained. It may be noted that we have used a pulsed injector in this experiment. With a modified injector design, whereby a continuous beam can be obtained, we hope to achieve higher n-doping levels.

In conclusion, we have been able to demonstrate very uniform and high levels of in situ n-type doping of silicon at low growth temperatures using supersonic jets of phosphine. Growth of uniformly doped thin films with electron mobilities close to bulk values has been achieved. p^+-n^+ and p^+-n^--n^+ diodes grown with such doping of the n-region show excellent electronic properties.

III. DEVICE STRUCTURE AND FABRICATION

The spectral response and impact ionization coefficients were determined from the measured photocurrents of p^+- $i(Si_{1-x}Ge_x)$-n^+ diodes ($0 \leq x \leq 1$) grown by molecular beam epitaxy (MBE) using Si_2H_6 (disilane) and solid Ge as sources[4]. Use of elemental Ge as a source material, rather than germane helped to maintain a stablized growth chamber pressure and provided better control of alloy compositions. The heterostructures were grown at temperatures ranging from 500 to

600°C. Prior to growth, the surface oxide was removed by heating the substrate to 840°C and a clear (2 x 1) reflection high energy electron diffraction pattern is observed. Figure 5(a) shows the schematic of a typical diode structure. The ~1μm $Si_{1-x}Ge_x$ i-region is undoped and the n- and p-type regions are doped with PH_3 and B, respectively. The alloy composition was determined from x-ray diffraction measurements on similar single layers grown under identical conditions. The carrier concentration profile of a typical diode, determined by spreading resistance analysis, is shown in Fig. 5(b). It is important to realize that the $Si_{1-x}Ge_x$ layers in the diodes are not pseudomorphic, but relaxed, and a misfit dislocation network is formed at the lower $Si/Si_{1-x}Ge_x$ interface. Mesa-shaped diodes, 500, 300 and 150 μm in diameter, were made by standard photolithography and reactive ion etching with a SF_6/O_2 mixture. Evaporated Al was annealed at 450°C to form ohmic contacts to both n- and p-regions. Typical measured reverse leakage currents were in the range of 20-170pA/μm^2 for reverse bias values between 4-12V. Figure 6 shows typical photocurrent and dark current-voltage chracteristics of a $Si_{1-x}Ge_x$ photodiode. Typical reverse leakage currents of pure Si diodes fabricated by the same method were in the range of 10-30pA/μm^2. The multiplication factors, discussed in Sec. IV, are measured from the photocurrent data by taking the ratio of the photocurrent to its unmultiplied value at low voltages.

IV. SPECTRAL RESPONSE CHARACTERISTICS

The external quantum efficiency can be expressed in terms of the responsivity as :

$$\eta = Rx\frac{hv}{q} \qquad (1)$$

where the responsivity $R = I_{ph}/P_{inc}$ and I_{ph} and P_{inc} are the measured photocurrent and incident optical power, respectively. η is dependent on the absorption coefficient of the material and in a real photodiode the short wavelength cut-off is determined by surface absorption and the long wavelength cut-off is determined by the absorption edge or bandgap of the semiconductor material. In the present work our objective was to characterize the long wavelength region of the spectral response of the $Si_{1-x}Ge_x$ photodiodes.

A variable wavelength light source in the spectral region of interest was provided by a high-power tungsten lamp and a combination of narrow bandpass filters. The light exiting from the filters was focussed onto the photodiode with the spot size made smaller than the device (mesa) diameter. The thickness of the top n+ SiGe layer (0.1 - 0.2μm) and that of the SiGe i-region (1 μm) ensured that most of the incident light was absorbed in the i-region and not in the Si substrate. The optical power absorbed in the devices was determined with a calibrated Ge photodiode at each wavelength, taking into account the reflectivity of the air/SiO_2 and $SiO_2/Si_{1-x}Ge_x$ interfaces of the top passivating SiO_2 layer. The signal-to-noise ratio in the measured photocurrent was inhanced with standard lock-in amplification with a chopper. The diodes were reverse biased at a value which was adequate for producing a reasonable photocurrent without the onset of any avalanche multiplication.

Figures 7(a)-(d) show the results of the spectral response measurements. The four figures show the responsivities, R, of $Si_{1-x}Ge_x$ photodiodes with compositions, x = 0.08, 0.31, 0.69 and 1.00 as a function of wavelength in the range 0.6 to 1.6μm. It is clear to see the long wavelength cut-offs of the responses increase as the Ge content in the i-region of photodiodes increases. They span the spectral region between 1.1-1.6μm, the Si and Ge bandgaps, as expected. It is also seen that the highest measured value of R of the photodiodes in this wavelength region is ~0.5A/W, which is

very reasonable and make these devices useful for all the applications mentioned earlier. It is to be noted that this is the responsivity without any multiplication.

V. IMPACT IONIZATION COEFFICIENTS

Photogenerated carriers in the active region of photodiodes travel at their saturation velocities and if they acquire enough energy from the field in the region to have ionizing collisions, they create secondary electron-hole(e-h) pairs and the process continues to produce carrier multiplication. We have deduced the impact ionization coefficients $\alpha(E)$ and $\beta(E)$ from the measured current multiplication factors in the $Si_{1-x}Ge_x/Si$ photodiodes. To inject pure electrons into the $Si_{1-x}Ge_x$ i-region of the p^+ - i - n^+ diodes, electron-hole pairs were generated by focusing a 488 nm Ar laser on the p^+ substrate of the mesa diodes. A lensed fiber was used to couple light into the devices. A Hewlett-Packard 4145B semiconductor parameter analyzer was used to bias the diodes and measure the current with and without illumination and thus determine the current multiplication. Pure hole injection in the same device was not possible because the top n^+ layer was not thick enough to absorb all the light at λ=488 nm. Similarly, it was not possible to inject pure electrons in a n^+ - i - p^+ diode. We have, therefore, determined both α and β from a single measurement of the electron multiplication factor M_n (or hole multiplication factor M_p) by using the equations outlined below.

Experimental results of impact ionization coefficients in Si and Ge show that Shockley's model[40] is applicable to these semiconductors. We therefore assumed the following forms of α and β in $Si_{1-x}Ge_x$:

$$\alpha(E) = \alpha o e^{-E_\alpha / E(x)} \tag{2}$$

and

$$\beta(E) = \beta o e^{-E_\beta / E(x)} \tag{3}$$

where α_o and β_o (cm^{-1}) are constant prefactors and E_α and E_β (V/cm) are constants. We denote $J_p(x)$ and $J_n(x)$ as the hole and electron currents at a point x in the depletion region of a *p-i-n* diode of width W, under high reverse bias. It is assumed that the electric field in the depletion region is in the positive x direction and pure electron current is injected at x = W. The total current $J(=J_p+J_n)$ is constant through the depletion region. The incremental electron current at x is given by

$$dJ_n(x) = J_n(x)\alpha(E)dx + J_p(x)\beta(E)dx \tag{4}$$

$$\frac{dJ_n(x)}{dx} = \alpha(E)J_n(x) + \beta(E)J_p(x) \tag{5}$$

Replacing $J_p(x)$ by $J-J_n(x)$ and solving this differential equation with the boundary condition $J_n(0)=J$, the electron multiplication factor M_n can be expressed as[16]:

$$1-\frac{1}{M_n} = \int_0^W \alpha(E)\exp[-\int_0^x (\alpha(E)-\beta(E))dx']dx \tag{6}$$

Similarly, for pure hole injection,

$$1-\frac{1}{M_p}=\int_0^W \beta(E)\exp[-\int_0^x(\beta(E)-\alpha(E))dx']dx \qquad (7)$$

The electric field profile E(x) is determined by solving the current continuity equation and Poisson equation simultaneously with the known carrier concentration profile in the i-region. Using equations 2 to 7, a non-linear equation with four unknowns, α_0, β_0, E_α and E_β, is formed :

$$1-\frac{1}{M_n}=\int_0^W F(\alpha_0,E_\alpha,\beta_0,E_\beta)dx \qquad (8)$$

We have taken the value of M_n at different bias voltages and formed a system of non-linear equations with four unknowns. We have deduced α_0, E_α, β_0 and E_β by a numerical curve fitting technique[41]. The value of M_p has been similarly derived.

Figure 8 shows the measured temperature-dependent current-voltage characteristics of a p^+-$i(Si_{0.69}Ge_{0.31})$-n^+ diode. The increase of the breakdown voltage V_{BR} with lowering of temperature confirms that avalanche multiplication is the dominant breakdown mechanism in these devices and that tunneling or the formation of microplasmas will not vitiate our results.

Figure 9(a) shows the results of measurements on a diode with a pure Ge i-region. The values of α and β are in fair agreement with published data for Ge[21-23]. This validates our measurement and analysis technique outlined above. Figure 9(b) depicts α(E) and β(E) measured in $Si_{0.69}Ge_{0.31}$. The measured α/β values as a function of x at E=330 KV/cm are listed in Table 2 and the coefficients themselves, at the same fixed value of E are shown in Fig. 10. The single most important feature in the data is that a crossover (α/β=1) occurs between x=0.4 and x=0.5. It is stressed that the values of α and β being reported here may be in slight error due to the uncertainty in the curve fitting process. However, the trend of the ratio α/β is as expected and is a very significant result for the $Si_{1-x}Ge_x$ alloys.

The measurements reported here have been made on relaxed alloys. Therefore, the misfit dislocation density in the active multiplication region is expected to be quite high (10^6-10^8 per cm^2). However, since we are measuring the properties of high energy carriers, the effect of dislocations on the impact ionization process is probably small. Secondly, in the relaxed alloys, the degeneracy in the bands is still present and only changes in E_g and alloy scattering affect the results. Therefore, an increase in the value of α with x is not expected[24], or observed, in our measurements.

VI. CONCLUSION

We have demonstrated the highest bevels of n-type doping in SiGe and Si with supersonic jet sources. The spectral response characteristics and carrier impact ionization coefficients have been measured in $Si_{1-x}Ge_xp^+$-i-n^+ photodiodes grown by MBE. The long wavelength cut-off of the photodiodes varies from 1.2μm to 1.6μm as x increases from 0.08 to 1.0. The maximum responsivity in the measured spectral region is ~0.5 A/W. The measured value of α/β varies from 3.3 at x = 0.08 to 0.3 at x = 1, agreeing reasonably well with published data from Si and Ge and

confirming for the first time that a cross-over occurs in the alloy system. This cross-over, for which $\alpha/\beta = 1$, occurs at $x \cong 0.45$.

REFERENCES

1. B. Meyerson, "UHV/CVD Growth of Si and Si:Ge Alloys: Chemistry, Physics, and Device Applications", in *IEEE,* pp. 1592-1602, 1992.

2. J. Bean, "Silicon Molecular Beam Epitaxy:1984-1986", *J. Cryst. Growth,* vol. 81, pp. 411-420, 1987.

3. J. Sturn, P. Scgwartz, E. Orubz, and H. Manoharan, "Growth of Si1-xGex by rapid thermal chemical vapor deposition and application to heterojunction bipolar transistors", *J. Vac. Sci, Technol.,* vol. B 9, pp. 2011-2016, 1991.

4. S. Li, P. Bhattacharya, R. Malik, and E. Gulari, "Molecular Beam Epitaxial Growth of $Si_{1-x}Gex$/Si Pseudomorphic Layers using Disilane and Germanium", *J. Electron. Mater.,* vol. 22, pp. 793-795, 1993.

5. S. Nelson, K. Ismail, J. Chu, and B. Meyerson, "Room-temperature Electron Mobility in Strained Si/SiGe Heterostructures", *Appl. Phys. Lett.,* vol. 63, pp. 367-369, 1993.

6. J. Lee, S. Li, J. Singh, and P. Bhattacharya, "Low-Temperature Photoluminescence of SiGe/Si Disordered Multiple Quantum Wells and Quantum Well Wires", *J. Electron. Mater.,* vol. 23, pp. 831-833, 1994.

7. S. Verdonckt-Vandbroek, E. Crabbe, B. Meyerson, D. Harame, P. Restle, J. Stork, and J. Johnson, "SiGe-Channel Heterojunction p-MOSFETs", *IEEE Trans. Electron Devices,* vol. 41, pp. 90-101, 1994.

8. S. Iyer, G. Patton J. Stork, B.S. Meyerson, and D. Harame, "Heterojunction Bipolar Transistor using SiGe Alloys", *IEEE Trans. Electron Devices,* vol. 36, pp. 2043-2064, 1989.

9. A. Pruijmboom, J. Slotboom, D. Gravesteijn, C. Fredriksz, A. van Gorkum, R. vad de Heuvel, J. van Rooij-Mulder, G. Streutker, and G. van de Walle, "Heterojunction Bipolar Transistor with SiGe Base Grown by Molecular Beam Epitaxy", *IEEE Electronic Device Letters,* vol. 12, pp. 357-359, 1991.

10. A. Gruhle, H. Kibbel, U. Konig, U. Erben, and E. Kasper, "MBE-Grown Si/SiGe HBTs with High β, f_T and f_{max}, *IEEE Electronic Device Letters,* vol. 13, pp. 206-208, 1992.

11. H. Temkin, T. Pearsall, J. Bean, R. Logan, and S. Luryi, "Ge_xSi_{1-x} strained-layer superlattice waveguide photodetectors operating near 1.3μm", *Appl. Phys. Lett.,* vol. 48, pp. 963-965, 1986.

12. H. Temkin, A. Antreasyan, N. Olsson, T. Pearsall, and J. Bean, "$Ge_{0.6}Si_{0.4}$ rib waveguide avalanche photodetectors for 1.3μm operation", *Appl. Phys. Lett.,* vol. 49, pp. 809-811, 1986.

13. T. Pearsall, "Si-Ge alloys and superlattices for optoelectronics", *Materials Science and Engineering,* vol. B9, pp. 225-231, 1991.

14. V. Kesan, P. May, E. Bassous, and S. Iyer, "Integrated waveguide-photodetector using Si/SiGe multiple quantum wells for long wavelength applications", in *IEEE IEDM Proceedings,* pp. 637-640, 1990.

15. R. McIntyre, "Multiplication noise in uniform avalanche diodes", *IEEE Trans. Electron Devices,* vol. ED-13, pp. 164-168, Jan. 1966.

16. G. Stillman and C. Wolf, *Semiconductors and Semimetals,* vol. 12, New York: Academic Press, 1977.

17. W. Grant, "Electron and hole ionization rates in epitaxial silicon at high electric fields", *Solid State Electron.,* vol. 16, pp. 1189-1203, 1973.

18. C. Lee, R. Logan, J.K.R.L. Batdorf, and W. Wierann, "Ionization rates of holes and electrons in silicon", *Phys. Rev.,* vol. 134, pp. A761-A773, 1964.

19. R.V. Overstraeten and H. Deman, "Measurement of the ionization rates in diffused silicon *p* - *n* junctions", *Solid State Electron.,* vol. 13, pp. 583-608, 1970.

20. E. Cartier, M. Fischetti, E. Eklund, and F. McFeely, "Impact ionization in silicon", *Appl. Phys. Lett.,* vol. 62, pp. 3339-3341, 1993.

21. D. Decker and C. Dunn, "Determination of germanium ionization coefficients from small-signal IMPATT diode characteristics", *IEEE Trans. Electron Devices,* vol. ED-1-7, pp. 290-299, 1970.

22. S. Miller, "Avalanche breakdown in germanium", *Phys. Rev.,* vol. 99, pp. 1234-1241, 1955.

23. B. Wul and A. Shotov, *Solid State Phy. Electron. Telecommun.,* vol. 1, p. 491, 1960.

24. K. Yeom, J. Hinckley, and J. Singh, "Theoretical study on threshold energy and impact ionization coefficient for electrons in $Si_{1-x}Ge_x$", *Appl. Phys. Lett.,* vol. 64, pp. 2985-2987, 1994.

25. R.A. Metzger and F.G. Allen, *J. Appl. Phys.,* **55**, 931 (1984).

26. J.C. Bean, *Appl. Phys. Lett.,* **33**, 654 (1978).

27. S.H. Li and P. Bhattacharya, *J. Appl. Phys.,* **76**, 2213 (1994).

28. B.S. Meyerson and B.L. Yu, *J. Electrochem. Soc.,* **131**, 2366 (1984).

29. M. Racanelli and D.W. Greve, *J. Vac. Sci. Technol. B,* **9**, 2017 (1991).

30. S.M. Jang, K. Liao and R. Reif, *Appl. Phys. Lett.,* **63**, 1675 (1993).

31. D.W. Greve, *Mater. Sci. Eng. B,* **18**, 22 (1993).

32. L.P. Chen, G.W. Huang and C.Y. Chang, *Appl. Phys. Let.,* **68**, 1498 (1996).

33. R. Malik, E. Gulari, S.H. Li, P. Bhattacharya and J. Singh, *J. Cryst. Growth,* **150**, 984 (1995).

34. R. Malik and E. Gulari, *Appl. Phys. Lett.,* **68**, 3156 (1996).

35. N. Maity, L.-Q. Xia, and J.R. Engstrom, *Appl. Phys. Lett.,* **66**, 1909 (1995).

36. H.S. Bennett, *Solid State Elec.,* **26**, 1157 (1983).

37. Landolt-Börnstein, *Numerical Data and Functional Relationships in Science and Technology,* New Series, Group III (Springer-Verlag, Berlin, 1989) vol. 22a.

38. S. Thomas, J. Fretwell, D. Kinosky, R. Qian, A. Mahajan, P. Munguia, S. Banerjee, A. Tasch and C. Magee, *J. Electron. Mat.,* **24**, 183 (1995).

39. A.S. Mauskar, H.A. Naseem, W.D. Brown and S.S. Ang, *J. Vac. Sci. Tech.,* **A11**, 1858 (1993).

FIGURE CAPTIONS

Figure 1: Bandgap change in $Si_{1-x}Ge_x$ with alloy composition *x*.

Figure 2: (a) SIMS doping profiles in Si, doped with phosphine from a supersonic injector at T_S=620°C for different injection pulse widths; and (b) phosphorus doping profiles obtained from spreading resistance analysis with phosphine injection at lower growth temperatures.

Figure 3: Doping level as a function of the substrate temperature measured by SRA. The dotted line is a guide to the eye.

Figure 4: Measured SRA doping profiles and current-voltage characteristics (inset) grown on p^+(100) Si with the n^+ doping achieved by supersonic injection of PH_3.

Figure 5: (a) *p^+(Si)-n^-(SiGe)-n^+(SiGe)* diode structure for pure electron injection, and (b) spreading resistance analysis data for the carrier concentration profile in a typical diode.

Figure 6: Photocurrent and dark current-voltage characteristics of a Ge/Si photodiode.

Figure 7: Spectral response of (a) $Si_{0.92}Ge_{0.08}$, (b) $Si_{0.69}Ge_{0.31}$, (c) $Si_{0.31}Ge_{0.69}$, and (d) Ge photodiodes.

Figure 8: Temperature dependent current-voltage characteristics of *p^+(Si)-i($Si_{0.69}Ge_{0.31}$)-n^+($Si_{0.69}Ge_{0.31}$)* photodiode.

Figure 9: (a) Measured impact ionization coefficients in Ge. The solid lines indicate previously published data (Refs. 19-21); (b) measured impact ionization coefficients in $Si_{0.69}Ge_{0.31}$.

Figure 10: Measured values of α and β as a function of Ge mole fraction in $Si_{1-x}Ge_x$ at E=330 KV/cm.

Table 1: Measured Hall electron concentrations and mobilities.

Tgrowth (°C)	Doping Level (x $10^{19}cm^{-3}$)		Hall mobility ($cm^2/V.s$)
	Hall	SRA	
620	1.2	1.2	126
575	3.0	3.8	118
550	4.1	5.0	90

Table 2: Measured values of α/β in $Si_{1-x}Ge_x$.

Composition (x)	α/β at E=330 KV/cm
0.00	10 - 2
0.08	3.3
0.30	1.7
0.68	0.3
1.00	0.75 - 0.25

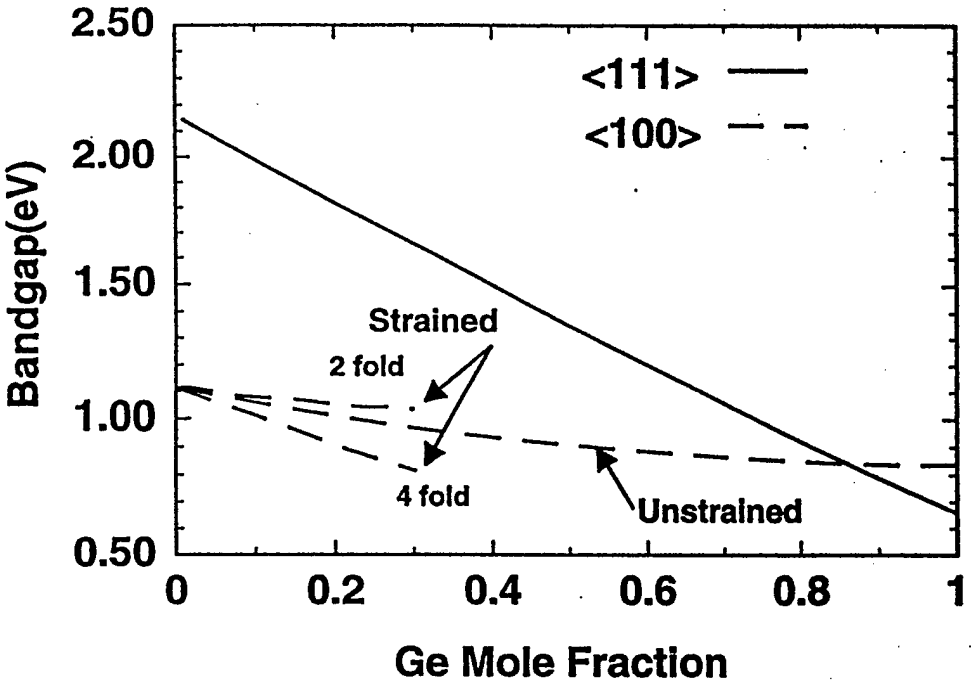
2.50
2.00
1.50
1.00
0.50
Bandgap(eV)
<111>
<100>
Strained
2 fold
4 fold
Unstrained
0
0.2
0.4
0.6
0.8
1
Ge Mole Fraction

Figure 1

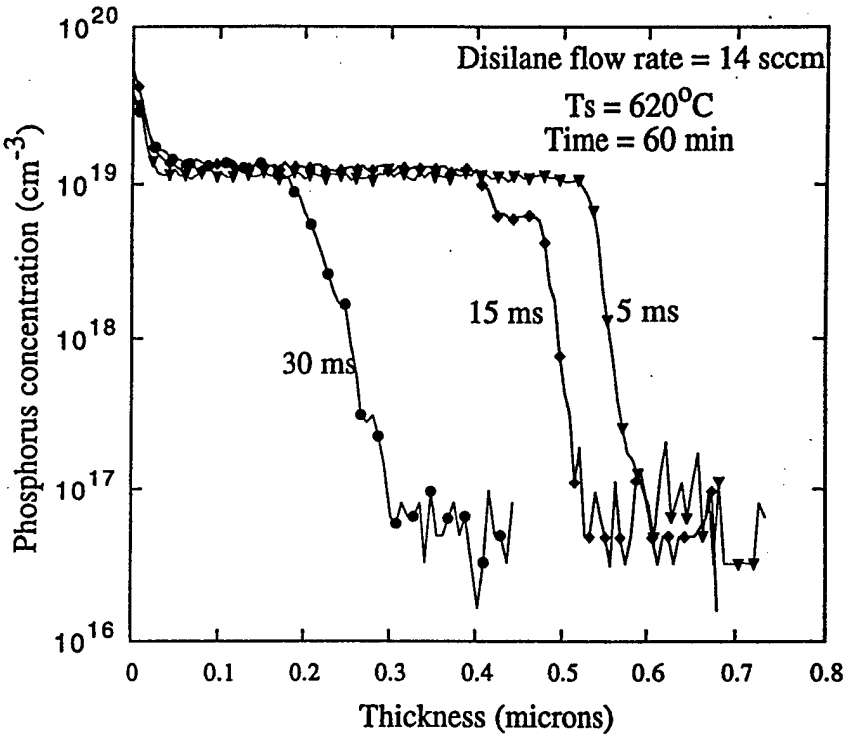
Disilane flow rate = 14 sccm
Ts = 620°C
Time = 60 min
30 ms
15 ms
5 ms
Phosphorus concentration (cm-3)
Thickness (microns)

(a)

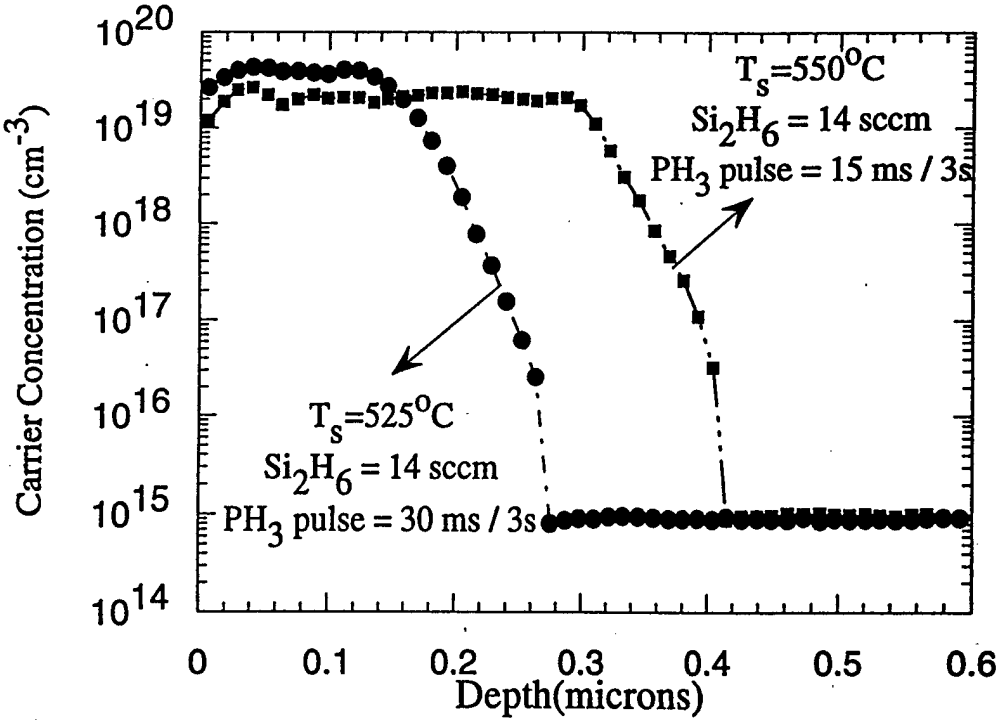
Ts=550°C
Si2H6 = 14 sccm
PH3 pulse = 15 ms / 3s
Ts=525°C
Si2H6 = 14 sccm
PH3 pulse = 30 ms / 3s
Carrier Concentration (cm-3)
Depth(microns)

(b)

Figure 2

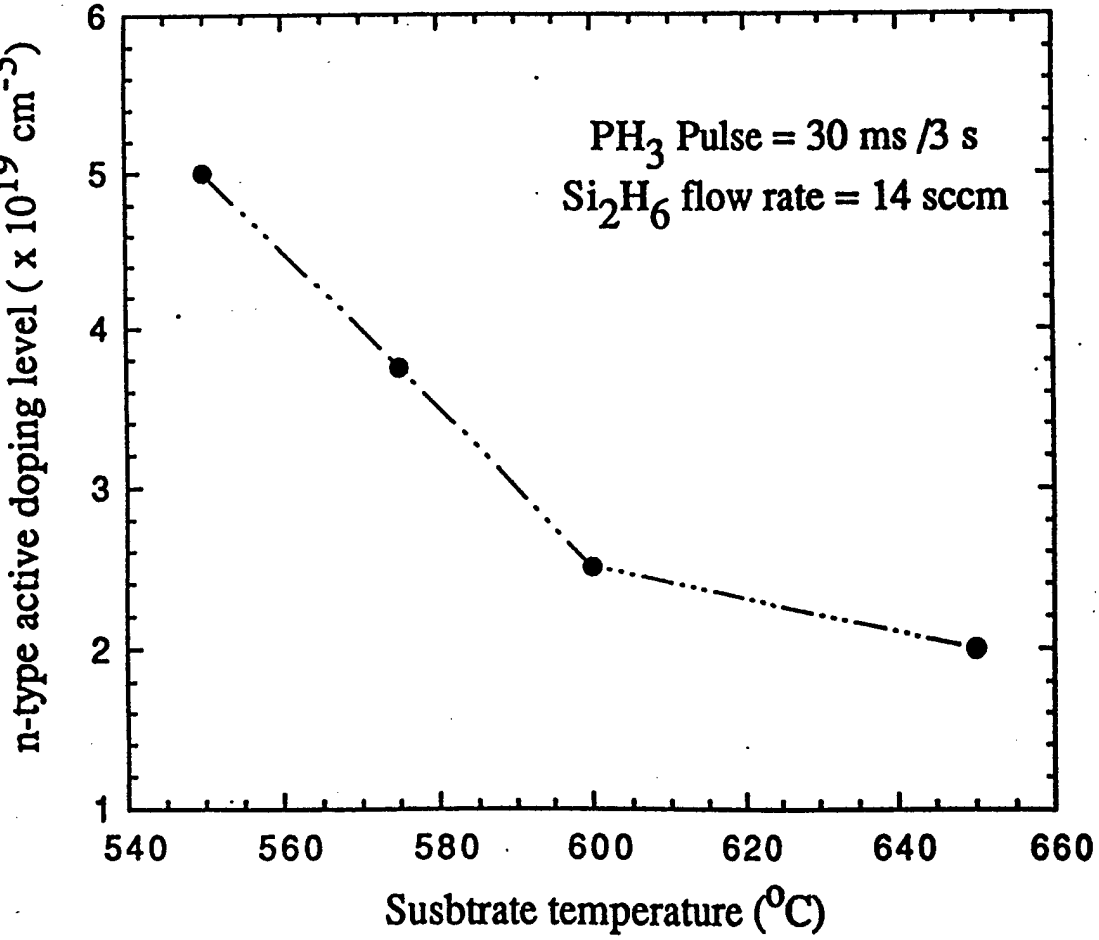
n-type active doping level (x 10^{19} cm^{-3})
6
5
4
3
2
1
540
560
580
600
620
640
660
Susbtrate temperature (^{o}C)
PH_3 Pulse = 30 ms /3 s
Si_2H_6 flow rate = 14 sccm

Figure 3

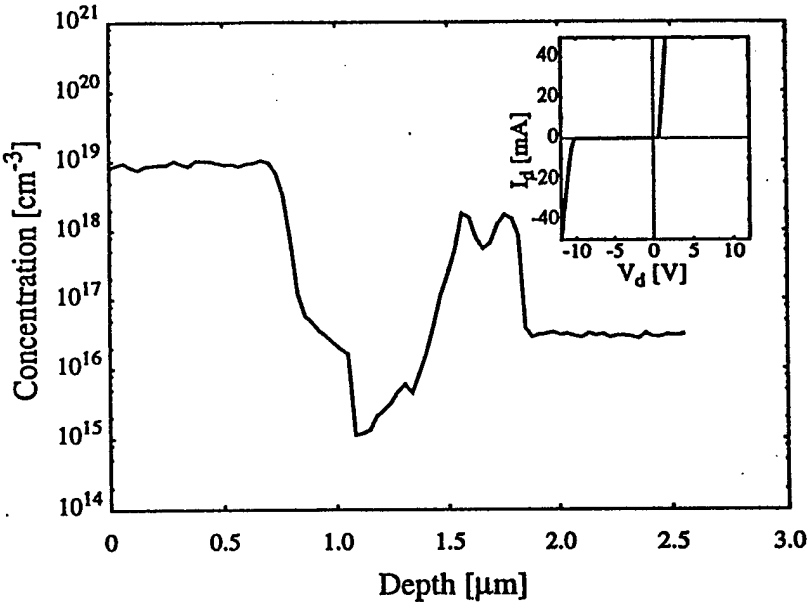
Concentration [cm^{-3}]
10^{21}
10^{20}
10^{19}
10^{18}
10^{17}
10^{16}
10^{15}
10^{14}
0
0.5
1.0
1.5
2.0
2.5
3.0
Depth [μm]
I_d [mA]
40
20
0
-20
-40
-10
-5
0
5
10
V_d [V]

(a)

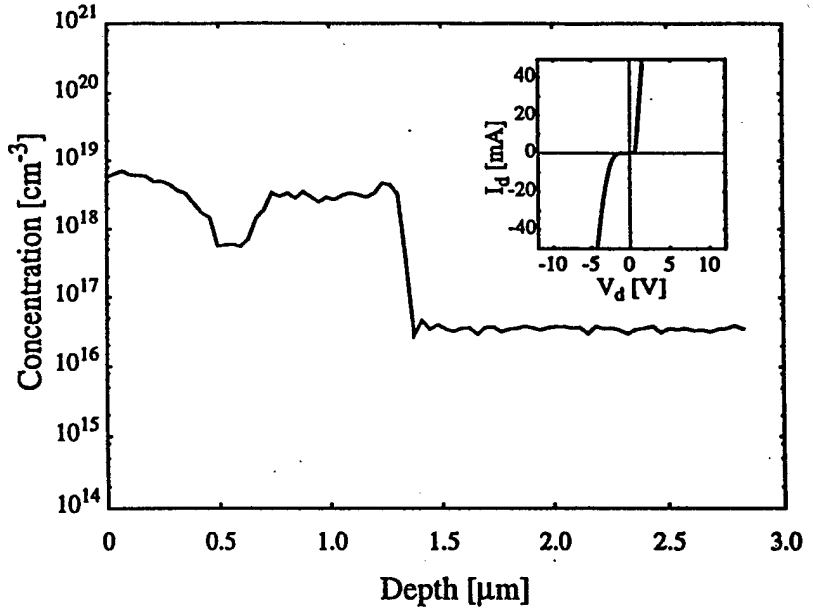
Concentration [cm^{-3}]
10^{21}
10^{20}
10^{19}
10^{18}
10^{17}
10^{16}
10^{15}
10^{14}
0
0.5
1.0
1.5
2.0
2.5
3.0
Depth [μm]
I_d [mA]
40
20
0
-20
-40
-10
-5
0
5
10
V_d [V]

(b)

Figure 4

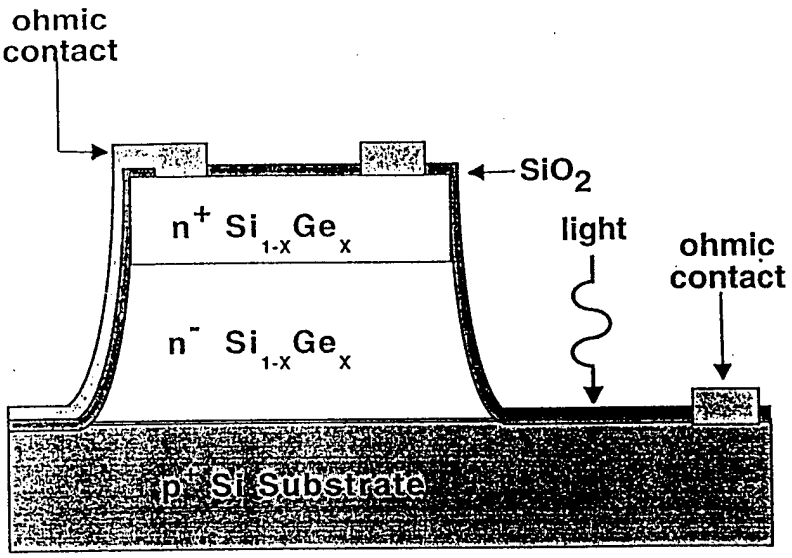
ohmic
contact
SiO_2
n^+ $Si_{1-x}Ge_x$
light
ohmic
contact
n^- $Si_{1-x}Ge_x$
p^- Si Substrate

(a)

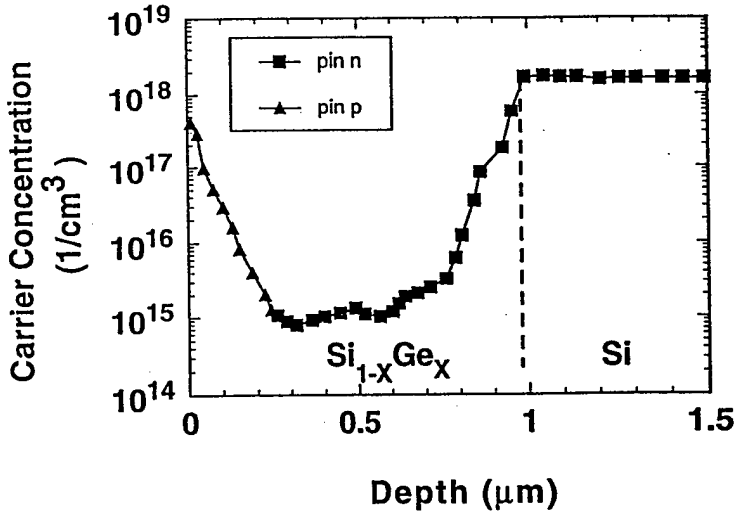
10^{19}
10^{18}
10^{17}
10^{16}
10^{15}
10^{14}
Carrier Concentration
$(1/cm^3)$
pin n
pin p
$Si_{1-X}Ge_X$
Si
0
0.5
1
1.5
Depth (μm)

(b)

Figure 5

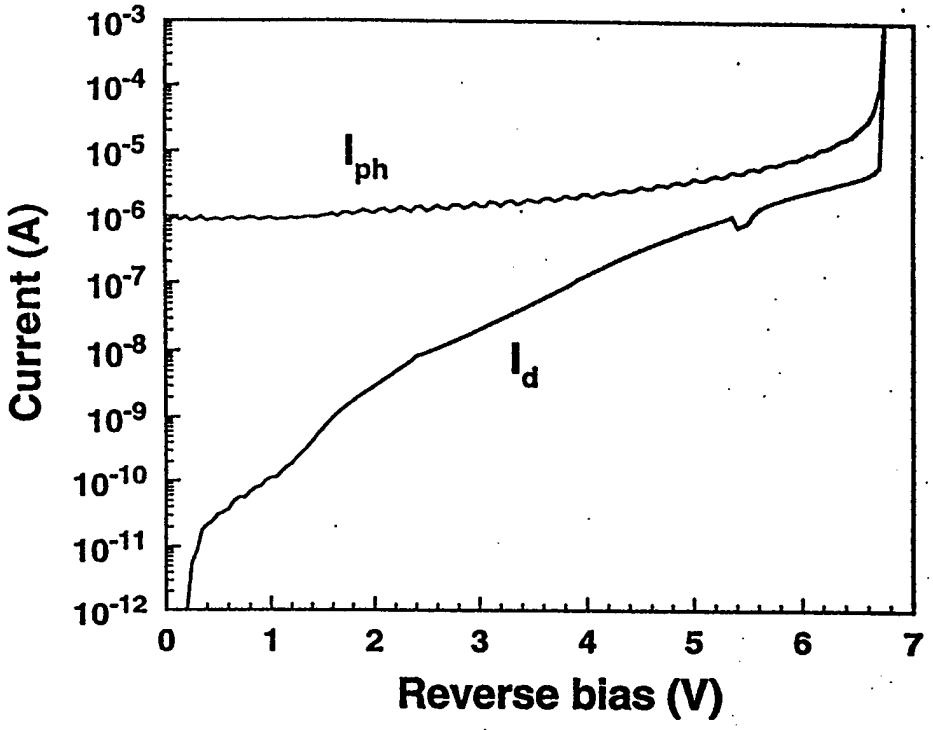
Current (A)
10-3
10-4
10-5
10-6
10-7
10-8
10-9
10-10
10-11
10-12
Iph
Id
0
1
2
3
4
5
6
7
Reverse bias (V)

Figure 6

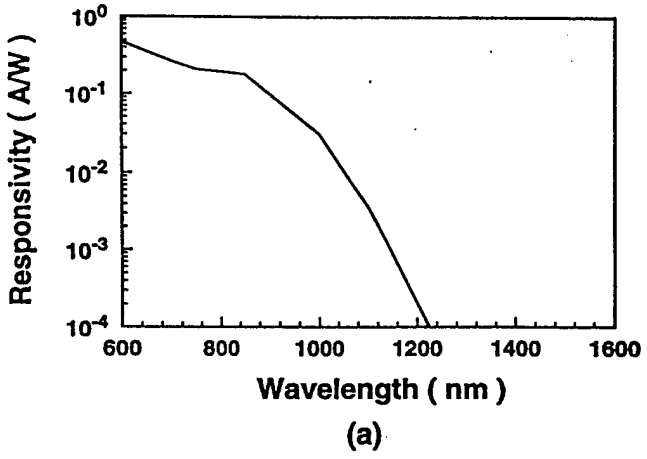

(a)

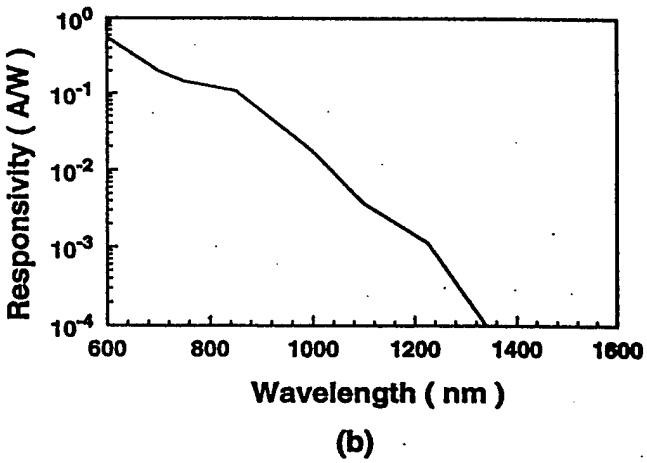

(b)

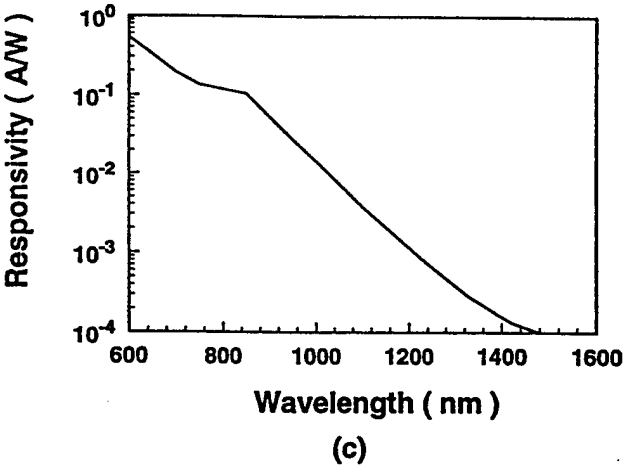

(c)

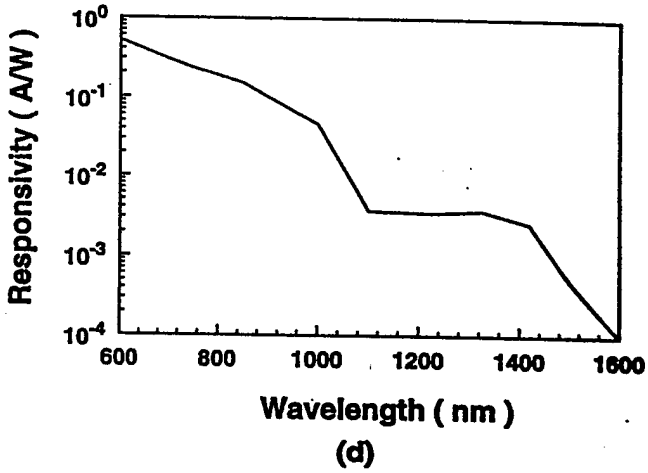

(d)

Figure 7

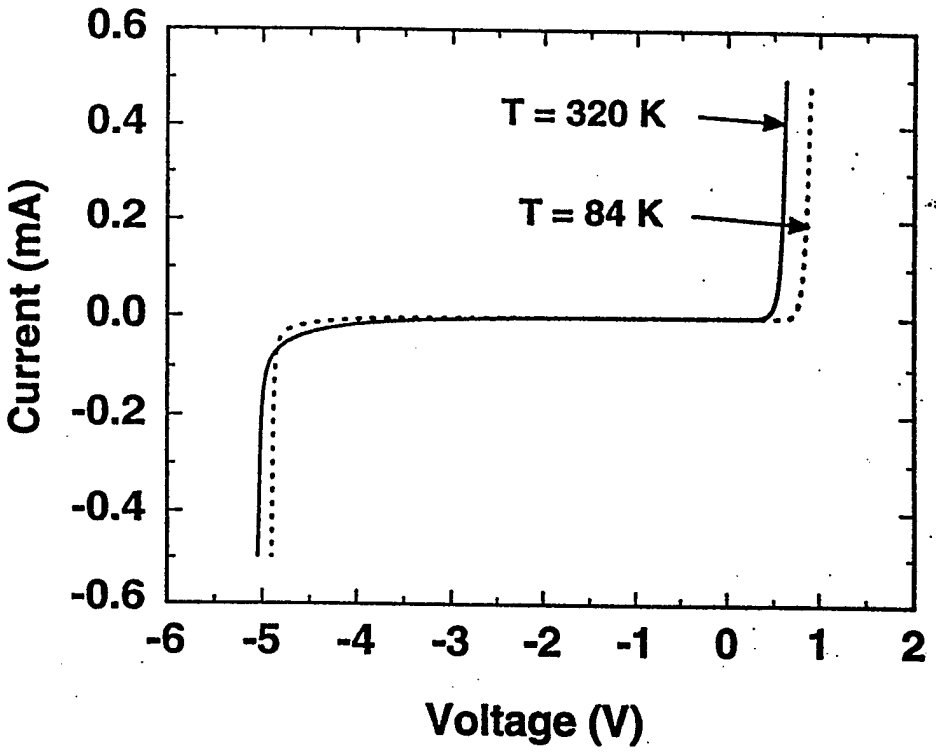

Figure 8

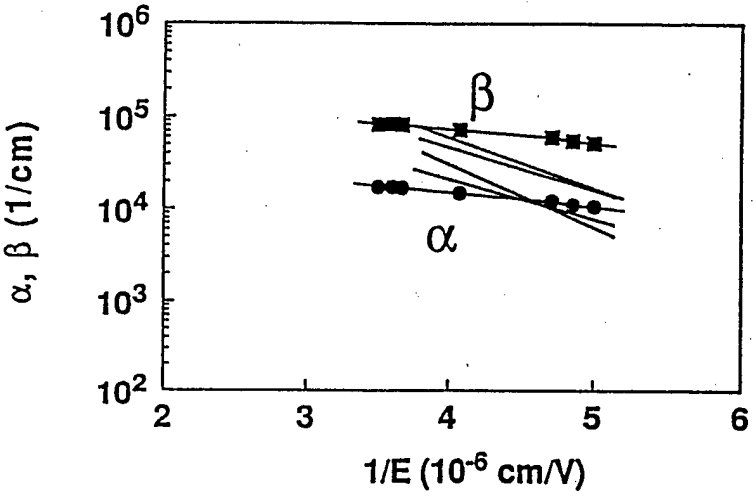
10^6
10^5
10^4
10^3
10^2
α, β (1/cm)
β
α
2
3
4
5
6
1/E (10^{-6} cm/V)

(a)

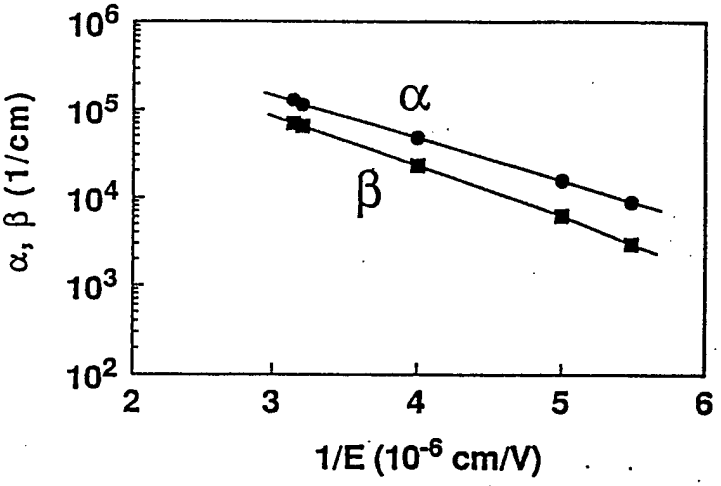
10^6
10^5
10^4
10^3
10^2
α, β (1/cm)
α
β
2
3
4
5
6
1/E (10^{-6} cm/V)

(b)

Figure 9

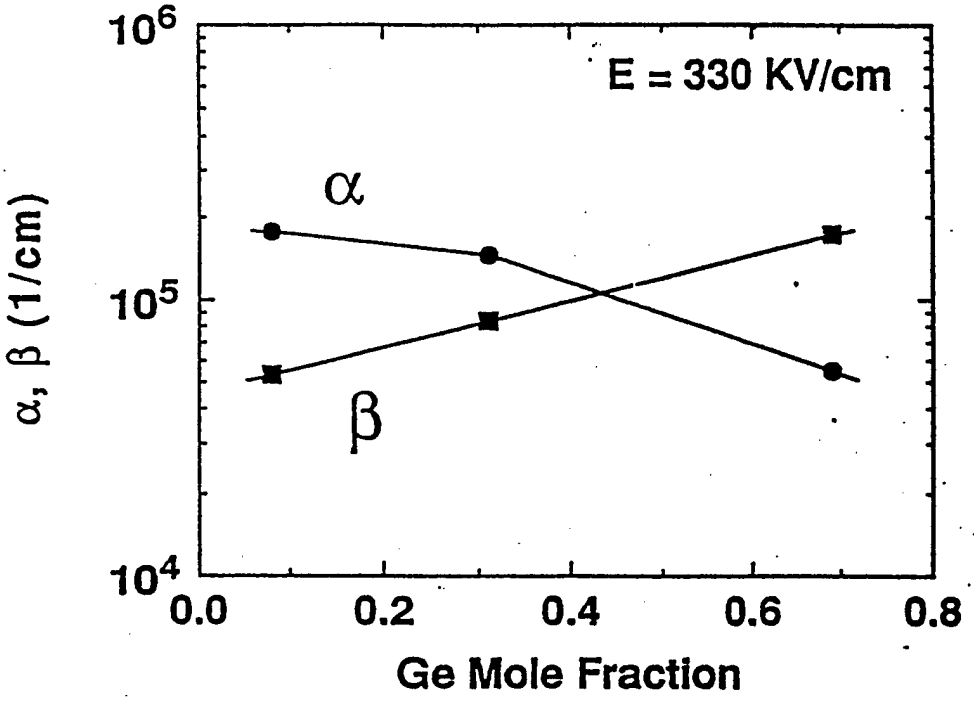

Figure 10